THE ASTROPHYSICAL JOURNAL, 382:523–529, 1991 December 1

10 MICRON SPECTRA OF PROTOSTARS AND THE SOLID METHANOL ABUNDANCE

W. A. SCHUTTE,[1] A. G. G. M. TIELENS,[2] AND S. A. SANDFORD[1]
Received 1991 March 25; accepted 1991 June 4

ABSTRACT

We have searched for the strong C-O stretching absorption of solid methanol near 9.8 μm toward the heavily obscured protostars AFGL 961, AFGL 2591, the BN object and Mon R2 IRS 3. There is no clear evidence for this feature in the spectra, resulting in very conservative upper limits to the methanol abundance of 6% to 17% relative to solid H_2O toward these objects. This is well below previous estimates of 50%–80% obtained toward W33 A, NGC 7538 IRS 9, AFGL 2136, and W3 IRS 5, which were based on the assignment of the interstellar 6.85 μm absorption feature to the methanol C-H bending mode. This study shows that such high methanol abundances are not a characteristic of all interstellar ices.

Subject headings: infrared: spectra — interstellar: grains — interstellar: molecules — stars: pre–main-sequence

1. INTRODUCTION

At the low dust temperatures inside dense clouds ($\sim$10 K) gaseous molecules are expected to accrete and react onto interstellar grains. In this way a dust grain is covered by an icy mantle consisting of such simple molecules as H_2O, CO, NH_3, and CH_3OH (Tielens 1989). The presence of absorption features at 3.08 and 4.67 μm due to H_2O and CO ice toward a large number of protostellar objects embedded in dense clouds as well as toward field stars which are obscured by dense cloud material confirms the existence of such mantles (Tielens & Allamandola 1987). Besides these bands, two adjacent absorption features at 6.0 and 6.85 μm have been observed in the protostellar sources W33 A, NGC 7538 IRS 9, AFGL 2136 and W3 IRS 5 (Soifer et al. 1979; Willner et al. 1982; Tielens & Allamandola 1987). While the 6.0 μm band can be identified with the OH bending mode of solid H_2O, the 6.85 μm feature has been ascribed to CH_3OH ice on the basis of a good spectral correspondence with laboratory ice samples (Tielens et al. 1984; Tielens & Allamandola 1987). The observed relative strengths of these features would indicate that the methanol abundance in interstellar ices is generally 50%–80% of H_2O, making it the most abundant ice constituent after H_2O (Tielens & Allamandola 1987). The presence of CH_3OH in the interstellar ices has been confirmed by the detection of a feature at 3.53 μm toward the heavily obscured protostar W33 A, which is fit very well by the laboratory spectrum of the C-H stretching mode of solid methanol. However, the relative strengths of the 3.53 and 6.0 μm bands indicates a CH_3OH/H_2O ratio of only $\sim$0.07 (Grim et al. 1991), almost a factor of 10 lower than inferred from the 6.85 μm band.

The discrepancy between the CH_3OH column densities indicated by the 3.53 and 6.85 μm features may be due to the presence of a reflection nebula associated with the disk geometry around the protostar. In that case, the photon path length through the nebula may be different at different wavelengths. That is, the near-IR photons may preferentially escape through the poles, while in the mid-IR they leave through the disk. In this way, longer wavelength absorption features could be enhanced substantially relative to shorter wavelength ones (Pendleton, Tielens, & Werner 1990). In this case, the best estimate for the CH_3OH/H_2O ratio is given by the 6.0 and 6.85 μm features. Alternatively, the bulk of the 6.85 μm feature may be due to species other than CH_3OH. For example, laboratory studies show that UV irradiation and warm up of astrophysical ice analogs containing NH_3 and CO produces a strong feature near 6.85 μm (Grim et al. 1989). A portion of the 6.85 μm band may also originate in carbonates (Puetter et al. 1979; Sandford & Walker 1985). Since these two possible interpretations of the discrepancy lead to widely different estimates of the importance of CH_3OH in interstellar ices, a solution would contribute considerably to our knowledge of the ice chemistry in dense interstellar clouds.

To better constrain the methanol abundance in interstellar ices, we have searched for additional absorption features. Figure 1 shows the spectrum of methanol ice after deposition at 10 K. The peaks and their assignments, as well as their peak cross section σ_{peak} and integrated cross section σ_{int}, are listed in Table 1. Besides the 3.53 (2830 cm^{-1}) and 6.85 μm (1460 cm^{-1}) C-H stretching and deformation modes, solid CH_3OH has a very strong feature near 9.8 μm (1020 cm^{-1}) due to the C-O stretching mode and a weaker adjacent one near 8.9 μm (1130 cm^{-1}) of the -CH_3 rocking mode. The peak optical depth of the 9.8 μm band is $\sim$5 times that of the 6.85 μm feature and more than 2 times that of the 3.53 μm one. The 8.9 μm feature has a peak optical depth similar to the 6.85 μm feature. In principle, the strengths of these features make them good candidates for detecting solid CH_3OH. Unfortunately, both features fall within the range of the strong interstellar silicate band. The exact profile of the silicate absorption feature is not well-known and in fact seems to vary from object to object (Willner et al. 1982), making it difficult to define a baseline relative to which the methanol feature should be measured. Moreover, the 9.8 μm feature falls within the region affected by atmospheric ozone. Nevertheless, in view of the large cross section of, in particular, the 9.8 μm band, it may still provide an important constraint on the solid methanol abundance.

This paper reports the results of a search for the 8.9 and 9.8 μm CH_3OH bands toward four heavily obscured protostellar objects AFGL 961, AFGL 2591, Mon R2 IRS 3, and BN. The paper is laid out as follows. In § 2 we describe the observational techniques and present our results. In § 3 we study the behavior of the 8.9 and 9.8 μm methanol features in various ice

[1] Space Science Division, NASA/Ames Research Center, MS:245-6, Moffett Field, CA 94035.
[2] Space Science Division, NASA/Ames Research Center, MS:245-3, Moffett Field, CA 94035.

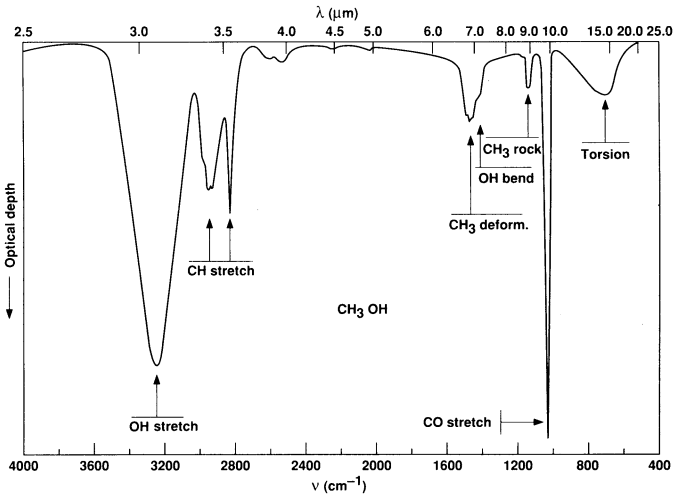

FIG. 1.—Infrared absorption spectrum of solid CH_3OH at 10 K

environments, using this information in § 4 to obtain upper limits to the solid methanol abundance in interstellar ices, followed by a discussion of the astrophysical implications of our results.

2. OBSERVATIONS

Spectra between 8.5 and 10.6 μm of AFGL 961, AFGL 2591, the BN object, and Mon R2 IRS 3 were obtained between 1989 October 24 and 26 at the NASA Steward 60″ (1.5 m) telescope on Mount Lemmon, Arizona, using the Faint Object Grating Spectrometer (FOGS; Witteborn & Bregman 1984). The chopping frequency of the infrared signal was 10 Hz with a beam separation of 60″ N-S. The aperture was 12″ in diameter, while the spectral resolution was $\Delta\lambda/\lambda \approx 0.0067$. Wavelength calibration was achieved by repeated measurements of an internal blackbody source through a polystyrene filter. The stability of the wavelength setting is better than 0.2 times the detector wavelength spacing over a time scale of a few hours (Witteborn et al. 1989), i.e., about 0.01 μm for the resolution used in our observations. For flux calibration and optimal removal of telluric features each object was ratioed by two standard stars which, in general, were observed shortly before and after the object, using the equation

$$O = \frac{O_r}{[S_1/\mathrm{BB}_1]^{\alpha}[S_2/\mathrm{BB}_2]^{1-\alpha}}, \quad (1)$$

where O_r and O are the raw and the reduced spectrum of the object, respectively, S_1 and S_2 are two measurements of standard stars at different air masses, BB_1 and BB_2 are the appropriate blackbody functions for the standards, and α is chosen such that the air mass of the reduced spectrum equals 0. Table 2 gives the specifics of our observations for the objects and accompanying standard stars.

Some care must be taken when assuming blackbody spectral distributions for the standards. In particular the late-type stars β Peg and α Her are expected to show an absorption feature due to the stretching mode of the SiO molecule. Recent observations of β And and μ UMa (spectral classes M0 IIIa and M0 III, respectively) show SiO features at $\sim$8.3 μm of optical depth 0.13 and 0.15, respectively, extending from 7.5 to about 9.1 μm (Witteborn, Bregman, & Rank 1991). Using the relation between spectral type and the observed depth of the first overtone of the SiO stretching mode (Rinsland & Wing 1982), an SiO optical depth of about 0.16 would be expected for β Peg. Being of a later stellar type, an even stronger SiO feature would be expected for α Her. Earlier observations, however, did not show any SiO feature stronger than $\tau = 0.1$ in the spectrum of this object (Merrill & Stein 1976). Still, the SiO band may somewhat influence our spectrum of AFGL 2591 for $\lambda = 9.1$ μm. It must be noted, however, that the feature does not extend within the wavelength range involved in our estimate of the strength of the methanol 9.8 μm feature (§ 4).

Unfortunately, only limited data are available on the spectra of our standards or comparable stars for $\lambda \geq 9$ μm. Moderate resolution data of α Her ($\Delta\lambda/\lambda = 0.015$) did not show any structure in excess of $\tau \approx 0.1$ between 8–13 μm. Furthermore, low-resolution data ($\Delta\lambda/\lambda = 0.02$) of α Boo, a K1 III star, did not show absorption features above a detection limit of $\tau \approx 0.14$ for 9 μm $\leq \lambda \leq$ 12 μm (Gillett, Low, & Stein 1968). It thus seems that the blackbody approximation could hold rather well longward of 9 μm. Additional high-resolution spectroscopy of standards in the 10 μm region is, however, desirable.

3. THE 8.9 AND 9.8 MICRON METHANOL BANDS

We have investigated the dependence of the shape and position of the methanol -CH_3 rocking mode near 8.9 μm and the C-O stretching mode near 9.8 μm on the ice composition and temperature. Two ice mixtures consisting of CH_3OH/H_2O = 0.05 and 0.67 (in keeping with general cocktail terminology henceforth the weak and the strong mixture, respectively) were deposited on a cold ($\sim$10 K) substrate followed by gradual warm-up. These mixtures represent two extreme situations for

TABLE 1

THE INFRARED ABSORPTION FEATURES OF SOLID METHANOL[a]

Vibratory Mode	ν (cm^{-1})	FWHM (cm^{-1})	λ (μm)	FWHM (μm)	σ_{peak} (cm^2 molecule^{-1})	σ_{int} (cm molecule^{-1})	σ_{int} (cm^2 μm^{-1} molecule^{-1})
OH stretch	3254	240	3.073	0.23	4.8 (−19)	1.3 (−16)	1.2 (−19)
CH stretch	2942	110	3.388	0.13	1.7 (−19)	2.2 (−17)	2.5 (−20)
CH stretch	2827	30	3.537	0.04	1.9 (−19)	6.6 (−18)	8.3 (−21)
CH_3 deformation / OH bend	1460 / 1410	100	6.849 / 7.092	0.47	9.8 (−20)	1.2 (−17)	5.7 (−20)
CH_3 rock	1128	35	8.865	0.27	5.2 (−20)	1.7 (−18)	1.3 (−20)
CO stretch	1026	30	9.747	0.29	5.8 (−19)	1.8 (−17)	1.7 (−19)
Torsion	695	220	14.39	4.7	7.6 (−20)	1.8 (−17)	3.7 (−19)

[a] Peak assignments were taken from d'Hendecourt & Allamandola 1986. The integrated cross sections σ_{int} and peak cross sections σ_{peak} were deduced from the relative band areas and peak heights (Fig. 1), using σ_{int} = 1.8 (−17) cm molecule^{-1} for the CO stretching mode (d'Hendecourt & Allamandola 1986) for conversion to absolute values.

TABLE 2

LOG OF OBSERVATIONS

Object	Standard Stars	Spectral Type	Observation Date	U.T.	Air Mass	Integration Time (minutes)
	α Her	M5 Ib	1989 Oct 24	02^h00^m	1.57	5
AFGL 2591			1989 Oct 24	03 30	1.22	12
	β Peg	M2.5 II	1989 Oct 24	03 52	1.02	5
	α Aur	G5 IIIe	1989 Oct 24	10 40	1.06	5
BN			1989 Oct 24	11 50	1.33	18
	α Aur	G5 IIIe	1989 Oct 24	13 00	1.20	5
	α Tau	K5 III	1989 Oct 26	10 54	1.10	5
Mon R2 IRS 3			1989 Oct 26	11 16	1.27	15
	α Tau	K5 III	1989 Oct 26	12 25	1.34	5
AFGL 961			1989 Oct 26	12 02	1.15	16
	α Tau	K5 III	1989 Oct 26	12 25	1.34	5
	α Tau	K5 III	1989 Oct 26	13 30	1.72	5

the methanol abundance proposed for the ices in interstellar space (§ 1).

Figure 2 shows the position of the features for the two mixtures after the deposition at 10 K, and after warm-up to 80 K and 120 K. At 10 K the C-O feature falls at 9.824 μm (1018 cm^{-1}) for the weak and at 9.726 μm (1028 cm^{-1}) for the strong mixture. Further studies show that the peak position of the C-O mode gradually shifts to shorter wavelengths once the CH_3OH/H_2O ratio is increased above 0.15. For CH_3OH isolated in argon, the C-O stretching mode occurs at 9.675 μm (1034 cm^{-1}; Serrallach, Meyer, & Günthard 1974). The C-O feature of the strong mixture has a long wavelength shoulder which probably corresponds to the band in the weak mixture (i.e., more isolated CH_3OH molecules). The feature of the weak mixture is narrower, with FWHM equal to 0.22 (46 cm^{-1}) compared to 0.28 μm (60 cm^{-1}) for the strong mixture.

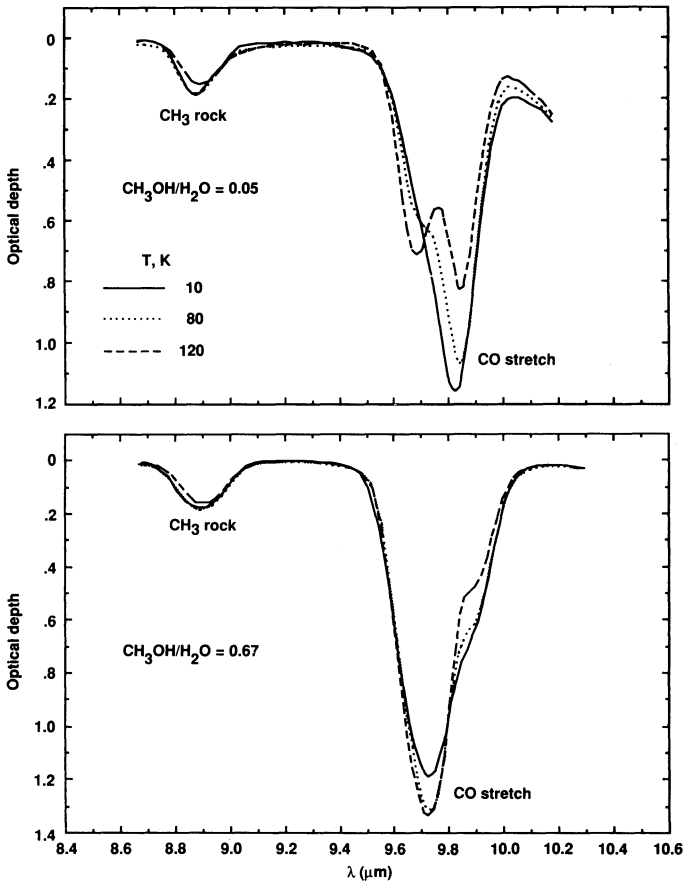

FIG. 2.—8.9 and 9.8 μm absorption features due to the methanol -CH_3 deformation and C-O stretching mode, respectively, for the ice mixtures $CH_3OH/H_2O = 0.05$ ("weak"; *top*) amd 0.67 ("strong"; *bottom*). Spectra were obtained after deposition at 10 K, and after warm-up 80 and to 120 K.

During warm-up to about 80 K, the C-O stretching feature of the weak mixture shifts slightly to 9.843 μm (1016 cm^{-1}; Fig. 2). Between 80–130 K, a second peak grows in at 9.670 μm (1034 cm^{-1}). In this temperature range the amorphous H_2O ice anneals gradually (Hagen, Tielens, & Greenberg 1981) and this peak therefore is likely due to methanol embedded in more annealed H_2O ice. At 120 K its peak depth is comparable to that of the 9.834 μm feature (Fig. 2). During the growth of the 9.670 μm peak, the integrated optical depth of the combined methanol feature decreases somewhat. The C-O feature of the strong mixture changes little upon warm-up, only its width has decreased somewhat at 120 K (Fig. 2), while the depth of the feature has slightly increased.

In contrast to the C-O stretching feature, the -CH_3 rocking band near 8.9 μm shows little dependence on ice composition and temperature. After deposition it is found at 8.881 μm (1126 cm^{-1}) in the weak and at 8.894 μm (1124 cm^{-1}) in the strong mixture. The feature starts to shift slightly once the ice is heated above 100 K, e.g., at 120 K it is found at 8.897 μm (1124 cm^{-1}) in the weak and at 8.905 μm (1123 cm^{-1}) in the strong mixture.

Summarizing, the peak of the C-O stretching band of interstellar solid methanol is expected to fall in the region 9.73–9.84 μm, depending on the CH_3OH concentration in the ice. At high temperatures, a second peak due to methanol inside annealed H_2O ice may develop at 9.67 μm. The maximum extension of the C-O stretching feature on the short-wavelength side is about 9.50 μm, and on the long wavelength side equals ~10.05 μm. The peak of the -CH_3 rocking mode is expected to fall between 8.88 and 8.90 μm while the feature extends between 8.73 and 9.02 μm.

4. DISCUSSION

The new spectra of the protostellar sources are shown in Figure 3. The spectra are generally dominated by the broad

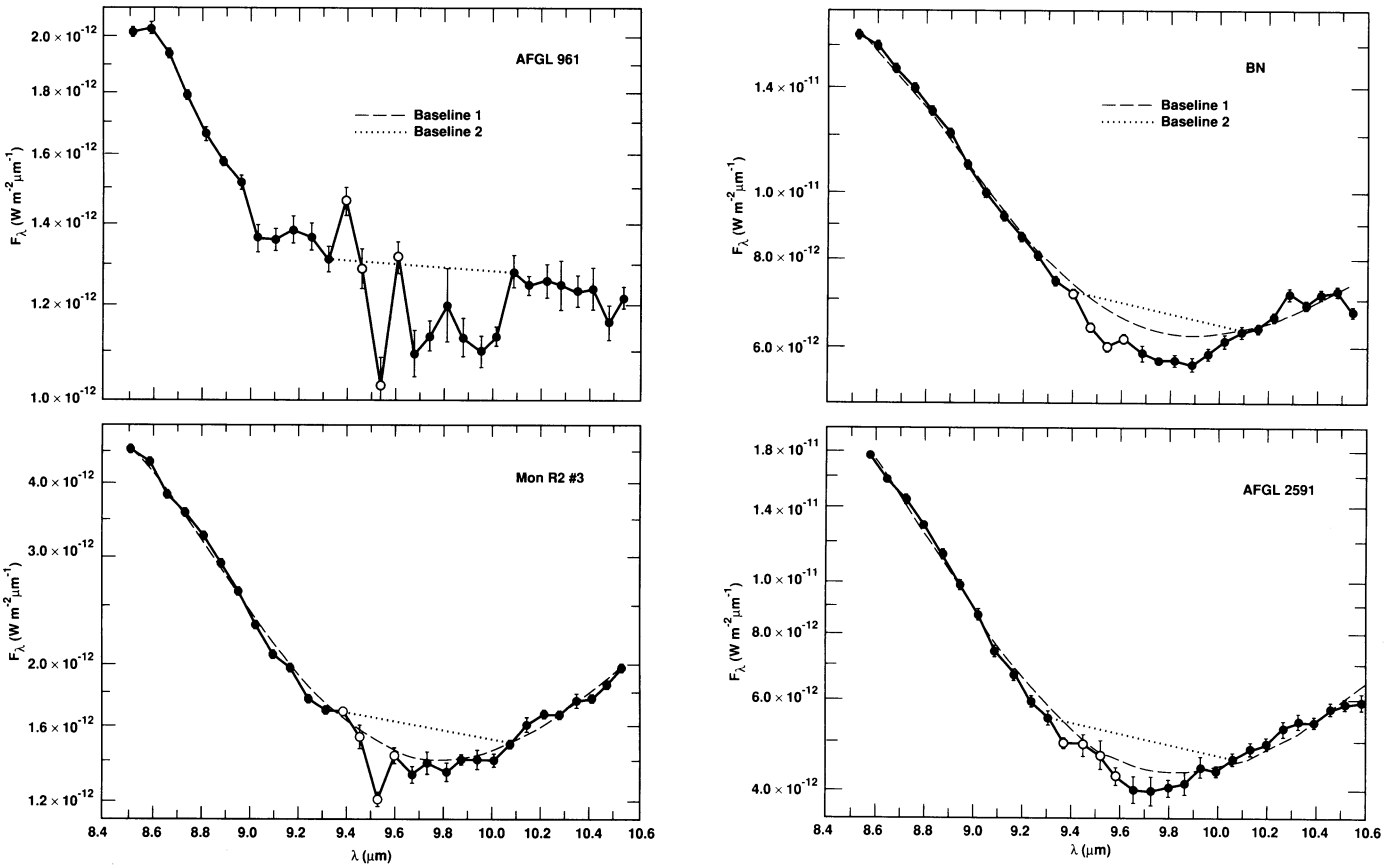

FIG. 3.—8.5–10.6 μm spectra of AFGL 961, the BN object, Mon R2 IRS 3, and AFGL 2591 as obtained with the NASA Steward 60″ telescope. Data points in the 9.35–9.63 μm region dominated by telluric ozone, are indicated by open circles. Baselines obtained by fitting the silicate feature using Trapezium type dust emissivities are indicated by a dashed line ("baseline 1"). Baselines used to obtain strict upper limits to the solid CH_3OH abundance are indicated by a dotted line ("baseline 2"). For details, see text.

silicate absorption feature. Within the errorbars, the silicate feature generally appears to be quite smooth, with the exception of the region between 9.35 and 9.63 μm. This corresponds to the center of the telluric ozone feature and the structure is likely due to incomplete correction for this band (see § 4.1).

The position and shape of the 9.8 μm methanol band depend on the ice temperature and the methanol concentration (§ 3). From the observed shape of the 3 μm H_2O band, which reflects the extent to which the ice has been annealed, ice temperatures ranging from $\sim$20 to $\sim$80 K have been inferred toward a variety of protostellar objects, while in some cases a small fraction of the ice may even be warmer (Smith, Sellgren, & Tokunaga 1989). Moreover, the CH_3OH concentration might be as low as $\sim$5% or as high as $\sim$80% relative to H_2O (§ 1). Due to these uncertainties, we should, in deducing (upper limits to) the CH_3OH abundance, integrate over the entire region in which the C-O stretching mode may absorb, i.e., from 9.50 to 10.05 μm.

Two problems complicate the assessment of the strength of the 9.8 μm methanol feature. First the presence of the telluric ozone band in the integration region could lead to the introduction of spuriour structure. Second, the definition of a baseline is complicated by the uncertainty in the shape of the silicate absorption feature, which underlies the potential CH_3OH absorption. These problems will now be discussed in turn before the abundance of CH_3OH is assessed.

4.1. *Telluric Ozone*

Atmospheric ozone has a strong absorption feature extending from 9.35 (1070 cm^{-1}) to 10.05 μm (995 cm^{-1}) which totally overlaps the 9.8 μm methanol band (Fig. 4). Imperfect cancellation of this absorption will introduce spurious structure at

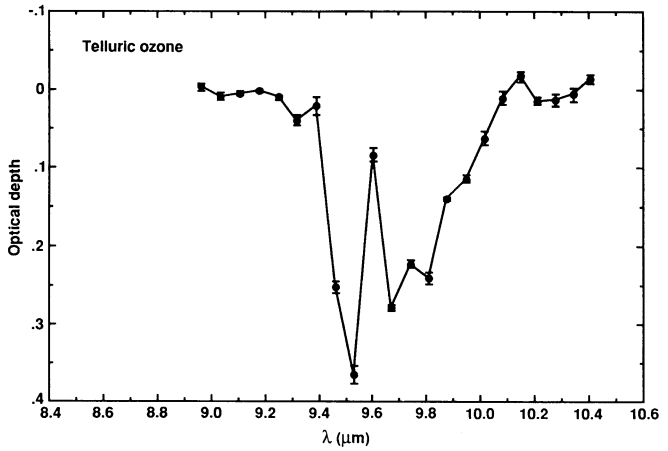

FIG. 4.—Telluric ozone absorption feature obtained by ratioing two measurements of the standard star α Tau with an air mass difference $\Delta A = 0.61$.

the position of the methanol feature. The appearance of structure in the spectra of the protostars in particular between 9.35 and 9.63 μm (1040 cm^{-1}; Fig. 3), is likely due to such incomplete correction. This is probably caused by variations in the profile of the ozone failure, since shifts of the spectrometer wavelength setting over time should be too small to explain the amount of structure observed in this region (§ 2). No such structure is obvious longward of 9.63 μm, indicating a more successful correction for the part of the telluric ozone band falling in the 9.63–10.05 μm region. Since even in the most extreme cases, no more than 15% of the absorption of the 9.8 μm CH_3OH feature falls shortward of 9.63 μm (see Fig. 2), we can estimate the integrated optical depth of the methanol band by integrating exclusively longward of 9.63 μm, thus avoiding the confused region between 9.35 and 9.63 μm.

To estimate the error introduced in the integration by the telluric ozone, we studied the (small) variation of the integrated optical depth per unit air mass of the fraction of the ozone band that falls between 9.63–10.05 μm by dividing the various pairs of standard stars by one another. We found that the integrated optical depth between 9.63 and 10.05 μm of ozone per unit airmass and its 1 σ variation equals $\tau_{int}(O_3)/A = 0.110 \pm 0.004$ μm (11.4 ± 0.4 cm^{-1}). Using equation (1), the 1 σ error in the integrated optical depth from 9.63 to 10.05 μm in the reduced protostellar spectra is then given by

$$\sigma(\tau_{int}) \approx A(\text{object})\, \sigma\left[\frac{\tau_{int}(O_3)}{A}\right] \sqrt{1 + \alpha^2 + (1 - \alpha)^2}\,. \quad (2)$$

Equation (2) typically yields an error of $\sim 8 \times 10^{-3}$ μm (0.7 cm^{-1}), i.e., an average error of 2% in the flux level of the individual data points in this region. Thus, as this analysis shows, the ozone correction in the region 9.63–10.05 μm scales exceedingly well with air mass (i.e., eq. [1]).

4.2. *The Baseline*

The position of the baseline, relative to which the depth of the methanol 9.8 μm feature is to be estimated, depends on the shape of the silicate absorption band. As a first-order approximation we fitted a baseline through the observed silicate absorption using the method of Gillett et al. (1975), in which the emission is modeled by optical thin emission from warm background silicate dust with foreground absorption by cold, nonemitting silicate dust. A Trapezium-type emissivity curve is assumed for both the warm and the cold dust (Gillett et al. 1975). We varied the free parameters T_d, the warm dust temperature, and τ(9.7), the cold dust 9.7 μm optical depth, to obtain a least-squares fit to the observed spectrum. The region 9.35–10.05 μm, where telluric ozone and solid methanol have absorption features (see §§ 3 and 4.1), was not included in the fitting procedure. Table 3 lists for the various objects the values of T_d and τ(9.7) for which the best-fitting model curves were obtained. These curves are labeled "baseline 1" in Figure 3. For AFGL 961 no satisfactory fit to the observed silicate band could be obtained by this method, possibly because of additional strong absorption features due to ices (Cox 1989; d'Hendecourt & Jourdain de Muizon 1989) as well as the likely presence of the well-known infrared emission bands at 7.7 and 8.6 μm (Schutte, Tielens, & Sandford 1991).

To define the baseline, our simple model uses the emissivity of the dust observed toward the Trapezium nebula to fit the silicate band. However, the intrinsic shape of the silicate absorption varies with the composition as well as the mineralogy (cf. Mg–rich vs. Fe–rich, olivine vs. pyroxene, amorphous vs. crystalline, etc.) of the silicate components. The presence of crystalline silicates, for example, could produce some substructure on the feature (see Farmer 1974; Schutte et al. 1990). None of these factors is well-determined, and the silicate composition may in fact vary from source to source (Tielens 1991). The intrinsic profile of the silicate feature toward our sources could thus be significantly different from that of the trapezium dust, making the accuracy of the obtained baseline in the region of the solid methanol absorption uncertain. Of course, our simplified treatment of the radiative transfer in the dust surrounding the protostellar objects could produce errors as well. We therefore have defined an alternative, very conservative, baseline by drawing a straight line between the first data point shortward of 9.35 μm and the first point longward of 10.05 μm, i.e. the data points bordering the region of the solid methanol and telluric ozone absorptions (see §§ 3 and 4.1). These are displayed as "baseline 2" in Figure 3. Measuring the optical depth of the 9.8 μm CH_3OH band relative to this baseline should give strict upper limits to the methanol column density.

TABLE 3

WARM DUST EMISSION TEMPERATURES T_d AND COLD DUST OPTICAL DEPTHS AT 9.7 μm τ(9.7) YIELDING THE OPTIMUM FITS TO THE OBSERVED SILICATE ABSORPTION FEATURES

Object	T_d (K)	τ(9.7)
BN	395	3.15
Mon R2 IRS 3	290	4.00
AFGL 2591	350	4.40

4.3. *Upper Limits on the Solid* CH_3OH/H_2O *Ratio*

Although BN, AFGL 2591, and Mon R2 IRS 3 all show some absorption below the baseline 1 fit of the silicate feature (Fig. 3), we conclude that, given the uncertainties in the silicate profile, no methanol features are obvious in the spectra of the protostellar sources. Nevertheless, in the following we assume that any absorption below the adopted baseline is due to the 9.8 μm feature of solid CH_3OH. The apparent absence of the relatively weak 8.9 μm CH_3OH feature toward the four protostellar sources is consistent with the weakness of the 9.8 μm band. Because the constraints that can be set on the CH_3OH abundance are stronger using the latter feature, we will concentrate our further analysis on the 9.8 μm feature. Since we want to determine the abundance of solid methanol relative to other ice components, we will compare our measurements of the CH_3OH 9.8 μm feature with the 3 μm H_2O band previously detected in our sources (Smith et al. 1989).

To estimate the methanol abundance we integrate the optical depth associated with our two baselines between 9.63 and 10.05 μm (Fig. 3). The results are listed in Table 4. The quoted 1 σ errors result from the correction for atmospheric ozone (see § 4.1) and from the statistical error in the datapoints. In quantifying the H_2O ice abundance the peak optical depth of the observed 3 μm band is used rather than the integrated depth in order to avoid other absorption features which in some cases may contribute to the wings of this absorption (Smith et al. 1989). The results are listed in Table 4. Note that the maximum depth of the CH_3OH 9.8 μm feature allowed by the observations (Fig. 3) precludes that more than ~10% of

TABLE 4

ESTIMATED ABUNDANCES OF SOLID CH_3OH RELATIVE TO H_2O

Object	$\tau_{int}(9.8)$ Baseline 1 (μm)	$\tau_{int}(9.8)$ Baseline 2 (μm)	$\tau(6.85)$[a]	$\tau(3\ \mu m)$[b]	$\frac{n(CH_3OH)}{n(H_2O)}$ [c] Baseline 1	$\frac{n(CH_3OH)}{n(H_2O)}$ [c] Baseline 2	$\frac{n(CH_3OH)}{n(H_2O)}$ [d] "6.85 μm"
AFGL 961	...	$\leq(5.3\pm1.2)(-2)$	≤0.47	2.5	...	$\leq(5.6\pm1.2)(-2)$	$\leq9.0(-1)$
AFGL 2591	$(1.5\pm0.8)(-2)$	$\leq(5.7\pm0.8)(-2)$	≤0.13	0.9	$(4.4\pm2.3)(-2)$	$\leq(1.7\pm0.2)(-1)$	$\leq6.9(-1)$
BN	$(3.0\pm1.2)(-2)$	$\leq(4.9\pm1.2)(-2)$	≤0.26	1.8	$(4.3\pm1.8)(-2)$	$\leq(7.2\pm1.8)(-2)$	$\leq6.9(-1)$
Mon R2 ISR 3	$(1.2\pm0.7)(-2)$	$\leq(4.8\pm0.7)(-2)$	≤0.22	1.2	$(2.7\pm1.6)(-2)$	$\leq(1.1\pm0.2)(-1)$	$\leq8.5(-1)$

[a] The optical depth at 6.85 μm, from Tielens et al. 1984 and Willner et al. 1982.
[b] From Smith et al. 1989.
[c] Using $\sigma_{int}(9.8\ \mu m)/\sigma(3\ \mu m) = 0.38\ \mu m$ (see text).
[d] Using $\sigma(6.85\ \mu m)/\sigma(3\ \mu m) = 0.21$ (see text.

the depth of the 3 μm absorption feature in the protostellar sources is due to the methanol OH stretching feature at 3.07 μm (3250 cm^{-1}; see Fig. 1). The conversion of band strengths to relative abundances was made using $\sigma_{int}(CH_3OH, 9.8\ \mu m)/\sigma(H_2O, 3\ \mu m) = 0.38\ \mu m$, found for $H_2O/CH_3OH = 2{:}1$ ice after deposition at 10 K, where σ_{int} and σ are the integrated cross section per CH_3OH molecule and the peak cross section per H_2O molecule, respectively. This ratio is constant within 20% in binary mixtures for methanol concentrations between 5% and 67% relative to H_2O. Between 10 and 80 K the integrated cross section of the CH_3OH feature varies by less than 10% in our laboratory ice mixtures (Fig. 2), while the peak cross section of the H_2O band increases by $\sim$20% during warm-up to 80 K (Hagen et al. 1981). Thus, the systematic error that is introduced by the conversion due to the dependence of the H_2O and CH_3OH features on the precise conditions in the ice mantle is at most of the same order as the (1 σ) statistical errors quoted in Table 4.

For comparison, upper limits to the CH_3OH/H_2O ratio were deduced from the optical depth at 6.85 μm of the previously observed broad 6.3–8.0 μm absorption feature (Table 4; Willner et al. 1982; Tielens et al. 1984). To convert optical depths to relative abundances, we used $\sigma(CH_3OH, 6.85\ \mu m)/\sigma(H_2O, 3\ \mu m) = 0.21$, found for a $H_2O/CH_3OH = 2{:}1$ ice mixture at 10 K. For our sources the observed absorption cannot be fit by the methanol 6.85 μm feature, indicating that other species may contribute (Tielens & Allamandola 1987). Moreover, at least some of the sources are likely "contaminated" by the polycyclic aromatic hydrocarbon emission features at 6.2 and 7.7 μm, making the interpretation of the spectra as consisting of a continuum with superposed absorption bands questionable (Tielens 1989; Schutte et al. 1991). The upper limits based upon the 6.85 μm band are considerably higher than those obtained from the 9.8 μm feature, stressing the importance of the spectrographic data in the 10 μm region for constraining the interstellar solid methanol abundance.

4.4. *Astrophysical Implications*

Our best estimates of the CH_3OH/H_2O ratio based on the fit of the observed silicate features with Trapezium dust range from 0.03 to 0.04, while strict upper limits between 0.06–0.17 were obtained. It must be noted, however, that our observations could also be consistent with zero methanol abundance. Unfortunately, no measurements of the CH_3OH/H_2O ratio are presently available from the 3.53 μm band, and only upper limits are available from the 6.85 μm band for our sources. Nevertheless, we note that our results are consistent with the CH_3OH/H_2O ratio derived from the 3.53 μm band in W33 A ($\approx$0.07; Grim et al. 1991) but are much less than those derived from the 6.85 μm features in W33 A, NGC 7538 IRS 9, W3 IRS 5, and AFGL 2136 ($\approx$0.5; Tielens & Allamandola 1987). This suggests that the 6.85 μm band is actually dominated by species other than CH_3OH (see § 1), or, alternatively, that the CH_3OH/H_2O ratio is highly variable in dense clouds. Future observations in the 10 μm region for a larger set of objects may further reveal the importance of CH_3OH in interstellar ices. The lack of interference by telluric ozone will especially make the Infrared Space Observatory (ISO) quite suitable for detecting the CH_3OH 9.8 μm feature. If observed, the 9.8 μm feature may, due to its sensitivity to the environment (Fig. 2), yield important information on the physical and chemical conditions in the ice mantles.

We gratefully acknowledge Fred Witteborn and Jesse Bregman for their continuing support in developing the observational hardware and software as well as for their valuable advice about proper data reduction. We are furthermore indebted to Lou Allamandola and Jeffrey Lee for making their spectrum of solid CH_3OH available to us. We also thank Dana Backman for assisting with the data collection and Amara Graps for help with the data reduction. Finally, we want to acknowledge valuable suggestions made by the referee, S. Willner. This research was supported by NASA grant 199-52-12-04.

REFERENCES

Cox, P. 1989, A&A, 225, L1
d'Hendecourt, L. B., & Allamandola, L. J. 1986, A&AS, 64, 453
d'Hendecourt, L. B., & Jourdain de Muizon, M. 1989, A&A, 223, L5
Farmer, V. C., ed. 1974, Infrared Spectra of Minerals (London: Mineralogical Society)
Gillett, F. C., Forrest, W. J., Merrill, K. M., Capps, R. W., & Soifer, B. T. 1975, ApJ, 200, 609
Gillett, F. C., Low, F. J., & Stein, W. A. 1968, ApJ, 154, 677
Grim, R. J. A., Baas, F., Geballe, T. R., Greenberg, J. M., & Schutte, W. A. 1991, A&A, 243, 473
Grim, R., Greenberg, J. M., Schutte, W., & Schmitt, B. 1989, ApJ, 341, L87
Hagen, W., Tielens, A. G. G. M., & Greenberg, J. M. 1981, Chem. Phys., 56, 367
Merrill, K. M., & Stein, W. A. 1976, PASP, 88, 285
Pendleton, Y. J., Tielens, A. G. G. M., & Werner, M. W. 1990, ApJ, 349, 107
Puetter, R. C., Russell, R. W., Soifer, B. T., & Willner, S. P. 1979, ApJ, 228, 118
Rinsland, C. P., & Wing, R. F. 1982, ApJ, 262, 201
Sandford, S. A., & Walker, R. M. 1985, ApJ, 291, 838
Schutte, W. A., Tielens, A. G. G. M., Allamandola, L. J., Cohen, M., & Wooden, D. H. 1990, ApJ, 360, 577
Schutte, W. A., Tielens, A. G. G. M., & Sandford, S. A. 1991, in preparation
Serrallach, A., Meyer, R., & Günthard, Hs. H. 1974, Journal of Molecular Spectroscopy, 52, 94
Smith, R. G., Sellgren, K., & Tokunaga, A. T. 1989, ApJ, 344, 413
Soifer, B. T., Puetter, R. C., Russell, R. W., Willner, S. P., Harvey, P. M., & Gillett, F. C. 1979, ApJ, 232, L53
Tielens, A. G. G. M. 1989, in IAU Symp. 135: Interstellar Dust, ed. L. J. Allamandola & A. G. G. M. Tielens (Dordrecht: Kluwer), 239

Tielens, A. G. G. M. 1991, in IAU Coll. 126, Origin and Evolution of Interplanetary Dust, ed. A. C. Levasseur-Regourd (Dordrecht: Kluwer), in press
Tielens, A. G. G. M., & Allamandola, L. J. 1987, in Physical Processes in Dense Clouds, ed. G. E. Morfill & M. Scholer (Dordrecht: Reidel), 333
Tielens, A. G. G. M., Allamandola, L. J., Bregman, J., Goebel, J., d'Hendecourt, L. B., & Witteborn, F. C. 1984, ApJ, 287, 697
Willner, S. P., et al. 1982, ApJ, 253, 174
Witteborn, F. C., & Bregman, J. D. 1984, in Cryogenic Optical Systems and Instruments, ed. R. K. Melugin (Proc. SPIE, Vol. 509), 123
Witteborn, F. C., Bregman, J. D., & Rank, D. M. 1991, private communication
Witteborn, F. C., Bregman, J. D., Wooden, D. H., Pinto, P. A., Rank, D. M., Woosley, S. E., & Cohen, M. 1989, ApJ, 338, L9